Microburst Scale Size Derived from a Bouncing Packet Microburst Simultaneously Observed with the FIREBIRD-II CubeSats

Mykhaylo Shumko[1], John Sample[1], Arlo Johnson[1], Bern Blake[2], Alex Crew[3], Harlan Spence[4], David Klumpar[1], Oleksiy Agapitov[5], Matthew Handley[1]

[1]Department of Physics, Montana State University, Bozeman, Montana, USA
[2]Space Science Applications Laboratory, The Aerospace Corporation, Los Angeles, California, USA
[3]The Johns Hopkins University Applied Physics Laboratory LLC, Laurel, Maryland, USA
[4]Institute for the Study of Earth, Oceans, and Space, University of New Hampshire, Durham, New Hampshire, USA
[5]Space Sciences Laboratory, UC Berkeley, Berkeley, California, USA

Key Points:

- A bouncing packet microburst was simultaneously observed by the two FIREBIRD-II CubeSats on February 2nd, 2015.
- The lower limit of the microburst's latitudinal and longitudinal scale sizes at LEO was 28.8 ± 0.8 km and 38.5 ± 8.8 km, respectively.
- The microburst LEO scale sizes mapped to the magnetic equator are at least 504 ± 14 km radially, and 451 ± 103 km azimuthally.

Corresponding author: Mykhaylo Shumko, msshumko@gmail.com

Abstract

The FIREBIRD-II CubeSats simultaneously observed a bouncing packet microburst on February 2nd, 2015 during a small storm. It's latitudinal scale size is greater than 28.8 ± 0.8 km and the longitudinal scale size is greater than 38.5 ± 8.8 km is calculated in low earth orbit. Using the Tsyganenko 1989 magnetic field model, these scale sizes were mapped to the magnetic equator to get the radial and azimuthal scale sizes of at least 504 ± 14 km and 451 ± 103 km, respectively. The scale size is necessary to addreess the relative importance of microbursts in radiation belt electron losses, and to the scale sizes of whistler mode chorus waves. Lastly, the electron bounce period of the subsequent bounces was calculated and compared to analytical and numerical bounce times to validate numerous magnetic field models.

1 Introduction

The dynamics of radiation belt electrons are complex, and are driven by competition between source and loss mechanisms. A few loss mechanisms include radial diffusion [*Shprits and Thorne*, 2004], magnetopause shadowing [*Ukhorskiy et al.*, 2006], and pitch angle diffusion [*Selesnick et al.*, 2003; *Abel and Thorne*, 1998] due to plasma wave and Coulomb scattering. As described in [*Millan and Thorne*, 2007; *Thorne*, 2010] and references contained within, there are a variety of waves that cause pitch angle scattering, including EMIC waves, Plasmaspheric hiss, ULF waves, and whistler-mode chorus. Whistler-mode chorus predominantly occurs in the dawn sector [*Li et al.*, 2009] and it accelerates (scatters) electrons with large (small) equatorial pitch angles[*Horne and Thorne*, 2003]. It is currently believed that chorus waves are responsible for intense increases in electron precipitation flux termed microbursts.

Historically, microbursts were first termed by *Anderson and Milton* [1964] who used high altitude balloon observations. Few years later, *Oliven and Gurnett* [1968] used the Injun 3 satelite data to reveal that chorus waves and microbursts simultaneously occir. Since then, microbursts have been observed in Low Earth Orbit (LEO) with, e.g. SAMPEX [*Nakamura et al.*, 1995, 2000; *Blake et al.*, 1996; *Lorentzen et al.*, 2001a,b; *O'Brien et al.*, 2003, 2004; *Blum et al.*, 2015] and FIREBIRD [*Crew et al.*, 2016]. High altitude balloons also observe microbursts in the form of Bremsstrahlung X-rays [*Parks*, 1967; *Woodger et al.*, 2015; *Anderson et al.*, 2017]. Similar to chorus waves, microbursts predominantly occur in the dawn sector [*Lorentzen et al.*, 2001b]. Understanding microburst precipitation is important to radiation belt dynamics since they have been modeled and empirically estimated to deplete the relativistic electron population of the outer radiation belt on time scales of hours to a few days [*O'Brien et al.*, 2004; *Thorne et al.*, 2005; *Shprits et al.*, 2007].

An important parameter in the estimation of instantenous radiation belt electron losses due to microbursts is their scale size. *Parks* [1967] used X-ray imagers on high altitude balloons to estimate the microburst scale size from Bramstrulung X-rays to be 40 ± 14 km. In *Blake et al.* [1996], a bouncing packet microburst observed with SAMPEX was estimated to have a latitudinal scale size of "at least a few tens of kilometers", while *Blake et al.* [1996] concluded that typically they are less than a few tens of electron gyroradii in size. *Dietrich et al.* [2010] used SAMPEX along with ground-based VLF stations to conclude that microbursts have scale sizes less than 4 km.

Since February 1st, 2015, microbursts have been observed by the FIREBIRD-II pair of CubeSats (FU3 and FU4) in LEO. On February 2nd, 2015, *Crew et al.* [2016] reported a microburst with a scale size greater than 11 km. On the same day, a bouncing packet microburst was simultaneously observed on both spacecraft. The microburst decay was observed over the period of a few seconds, while the spacecraft were traversing in L. This analysis uses FU3 and FU4 to resolve the space-time ambiguity of the microburst. The rest of this paper is organized as follows: in section 2, the spacecraft and the microburst observation will be introduced. In section 3, the methodology of the spacecraft time and position correction,

the microburst latitudinal and longitudinal scale sizes in LEO and the magnetic equator, and electron bounce period will be explained. Lastly, in section 4, these results will be tied to the current empirical and theoretical understanding of microbursts and their connection to whistler-mode chorus scales.

2 Spacecraft and Observation

FIREBIRD-II is an identically-instrumented pair of 1.5 U CubeSats (FU3 and FU3), launched on January 31st, 2015. Their polar orbit has an apogee of 632 km and perigee of 433 km, and 99° inclination [*Crew et al.*, 2016]. FU3 and FU4 are flying in a leader-follower configuration with FU4 ahead, to resolve the space-time ambiguity inherent to single spacecraft missions such as SAMPEX.

Each FIREBIRD-II unit has a collimated and a surface solid state detector with complementary fields of view of 45° and 180°. They are observing electron precipitation in six energy channels from $\sim$ 230 keV to $>$ 1 MeV. The adjustable sampling rate is 18.75 ms by default and can be at a fast as 12.5 ms [*Crew et al.*, 2016].

On February 2nd, 2015 at 06:12:50 UT, a microburst with subsequent bounces was observed simultaneously on both spacecraft. Figure 1 shows the electron flux data (HiRes) of the microburst. Five peaks were observed on both spacecraft. On the collimted detector, the microburst was seen up to the fourth energy channel (555 - 771 keV), while on the surface detector it was observed up to the fifth energy channel (683 - 950 keV). Only FU3 has a functioning surface detector, thus only data from the lowest four energy channels of the collimated detectors will be used for this analysis. In addition, since FU4's 5th peak in the fourth energy channel is burried in Poisson noise, only the first four peaks were used in the spatial scale analysis.

The earliest peak is not dispersed, and subsequent peaks show dispersion, which implies that this is a single microburst with subsequent decaying bounces. At this time, the spacecraft was above Sweden, latitude = 63°, longitude = 15°, altitude = 650 km, at the eastern edge of the bounce loss cone (BLC). For this analysis, the BLC is defined as the region where an electron observed at FIREBIRD's altitude will mirror at an altitude less than 100 km in the opposite hemisphere, and could be lost due to collisions in the atmosphere [*Abel and Thorne*, 1998]. For locally mirroring electrons, the mirror point in the opposite hemisphere was calculated to be 95 km using the Tsyganenko 1989 (T89) magnetic field model [*Tsyganenko*, 1989] with the IRBEM library. The geomagentic conditions at the time were Kp = 4, and DST = -44 nT, during the transition between the main and recovery phases. Using the spacecraft location and geomagnetic conditions, the geomagnetic location at this time was McLlwain L = 4.7, MLT = 8.3, calculated using T89.

3 Analysis

3.1 Time and position correction

At the beginning of the FIREBIRD-II mission, their clocks were not synchronized and there was uncertainty in their separation. The approach to calculate their relative clock difference δt_e, is a cross-correlation time lag analysis on temporal events that are observed simultaneously, e.g. a train of identical microbursts seen on both spacecraft on the same day as the microburst in this case study.

Six time periods with coincident microbursts were hand-picked on February 2nd, 2015 for this analysis. The clock difference from the simultaneous microbursts were linearly fit to account for clock drift and a clock difference of $\delta t_e = 2.28 \pm 0.12\ s$ was calculated. This time shift was applied to the HiRes data in Fig. 1.

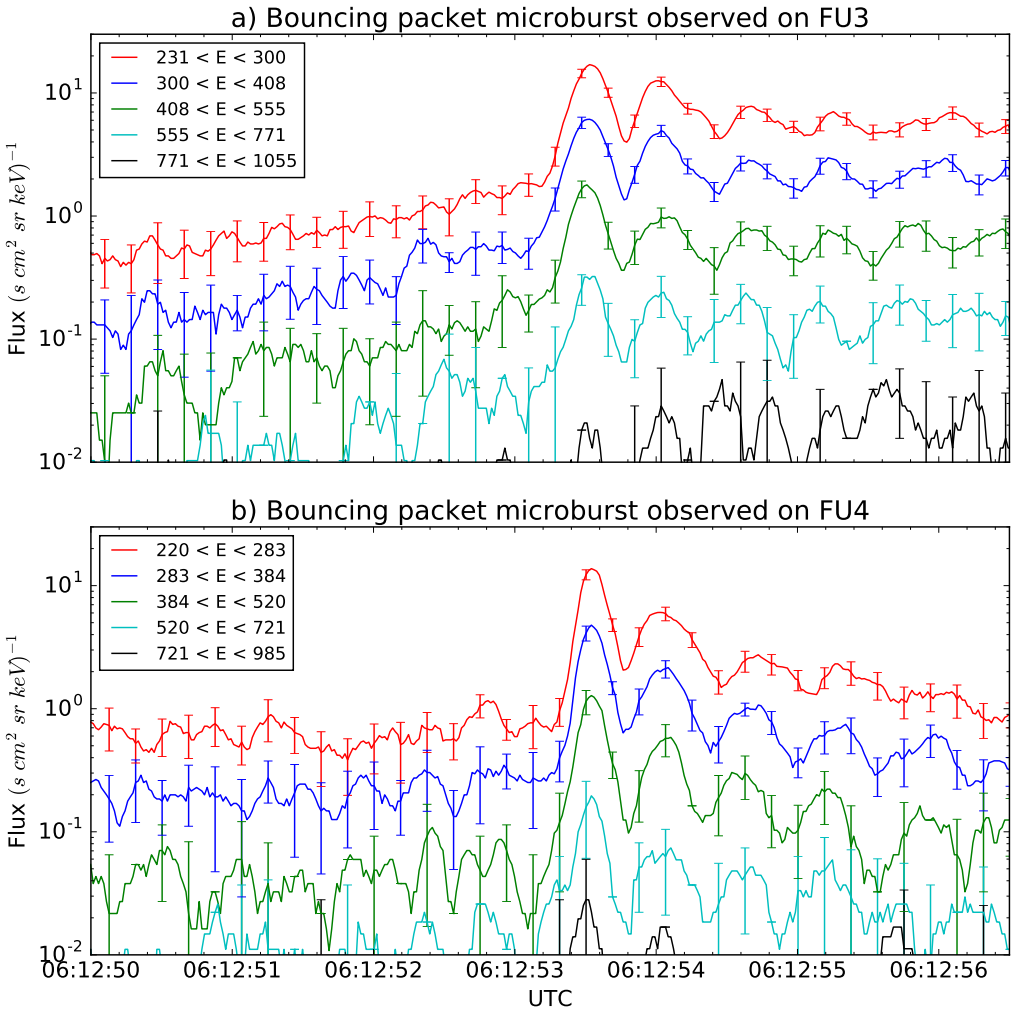

Figure 1. HiRes data of the microburst observed at February 2nd, 2015 at 06:12:50 UT, smoothed with a 150 ms window. The subsequent bounces show little energy dispersion. The energy channels' label unit is keV. As discussed in section 3 a time correction of -2.28 s has been applied to FU3. While the flux from five energy channels is shown, only channels with reasonable counting statistics are used for the spatial scale analysis.

To calculate their separation, the data was first corrected for the clock difference, and the same cross-correlation time lag analysis was applied on spatial events that are stationary. The observed spatial structures are believed to be stationary from similar structures observed with energies from > 35 keV to a few hundred keV on the AC-6 CubeSats while their position was confirmed with GPS [*Blake and O'Brien*, 2016]. This time lag, δt_d for the spatial events is the time it takes the trailing satellite to move to the leading satellite's position.

The cross-correlation analysis on the two spatial events yields a time lag of $\delta t_d = 2.64 \pm 0.12$ s. Using these values, and the Two Line Elements (TLE) derived spacecraft velocity, $v = 7.57\ km/s$ the calculated spacecraft separation was,

$$d = v\ \delta t_d = 19.9 \pm 0.9\ km. \tag{1}$$

An independent method to confirm the cross-correlation derived separation and timing difference was developed. The separation was calculated using TLEs. The TLE released for February 2nd, was anomalous and was not used. Instead, we backpropagated seven TLEs released up to five days after the microburst event, using the SGP-4 algorithm [*Hoots and Roehrich*, 1980]. Then the predicted spacecraft separations at the time of the microburst event were averaged to derive a separation of $d = 18.4 \pm 1.5$ km. The timing difference was calculated using the time stamps of the FIREBIRD-II telemetry beacons during operational passes. Since they had a common time reference, the ground station computer, a time difference $\delta t_e = 2.45^{+0.51}_{-0.98}$ s was derived. These two methods give similar results, which imply that the stationary event assumption used in the cross-correlation time lag analysis, is in fact, a reasonable assumption.

3.2 Microburst Scale Sizes

Using the event and orbit topology shown in Fig. 2 and error propagated from the spacecraft separation, the latitudinal scale size is greater than 28.8 ± 0.8 km. This scale size is represented by the latitudinal extent of the solid and dashed boxes in Fig. 2.

Since magnetospheric electrons drift eastward and were seen for multiple bounces, it is possible to calculate the longitudinal scale size of the microburst. The distance that the electrons drift azimuthally in a single bounce is given by,

$$d_{az} = 2\pi(R_E + A)\cos(\lambda)\frac{t_b}{< T_d >} \tag{2}$$

where R_E is the Earth's radius, A is the spacecraft altitude, λ is the magnetic latitude, t_b is the electron bounce period, and $< T_d >$ is the electron drift period. *Parks* [2003] derived $< T_d >$ to be,

$$< T_d > \approx \begin{cases} 43.8/(L \cdot E) & \text{if } \alpha_0 = 90^\circ \\ 62.7/(L \cdot E) & \text{if } \alpha_0 = 0^\circ \end{cases} \tag{3}$$

where E is the electron energy is MeV, L is the L shell, and α_0 is the equatorial pitch angle. The valid limit for this analysis is $\alpha_0 = 0^\circ$ since electrons mirroring at FIREBIRD-II have $\alpha_0 \approx 3.7^\circ$.

The microburst's longitudinal scale size is the furthest distance that its electrons drifted east and were last seen. This was calculated with $D_{az} = n\ d_{az}$ where n is the number of bounces observed. Using this methodology, the longitudinal scale size is greater than $38.5 \pm 8.8\ km$ for the 555 keV electrons shown as the red thin dashed box in Fig. 2 and greater than $50.8 \pm 11.4\ km$ for the 771 keV electrons shown as the red thick dashed box in Fig. 2. The stars with energy labels in Fig. 2 represent the locations of electrons with that energy when the microburst was seen at the first peak (P1), and drifted eastward to be last seen at P5 for FU3 and P4 for FU4.

The longitudinal and latitudinal scale sizes at LEO were mapped to the magnetic equator using the T89 magnetic field model. The radial scale size (latitudinal scale mapped from LEO) is greater than 504 ± 14 km and azimuthal scale size (longitudinal scale mapped from LEO) of 555 keV electrons is greater than 451 ± 103 km and of 771 keV electrons is greater than 530 ± 119 km.

3.3 Electron Bounce Period

Lastly, the observed bounce period, t_b as a function of energy is calculated. To calculate the observed t_b and uncertainties, the raw HiRes flux was detrended and fitted. The detrening flux (baseline) is defined in *O'Brien et al.* [2004] as the flux at the 10th percentile over a time interval around the point to be detrended. A 0.5 s interval is used in this analysis. The flux was fitted with five Gaussians for FU3, and four for FU4. The fit uncertainty is from the detrended flux and the baseline flux summed in quadrature. Using the fit parameters, the mean t_b for the lowest four energy channels was calculated and shown in Fig. 3 with rectangles.

The bounces observed with FU3 are biased to earlier times in the lowest two energy channels. This hints at the underlying distribution of electron flux within the energy channel and there are more electrons at the higher energy end of the channel. A Gaussian fit cannot account for this bias, and as a first order correction, minima between peaks was used to calculate t_b, and is shown in Fig. 3.

Superposed on Fig. 3, are t_b curves for various models including an analytical solution from *Schulz and Lanzerotti* [1974], and numerical models: T89, Tsyganenko 2004 (T04) [*Tsyganenko and Sitnov*, 2005], and Olson & Pfitzer Quiet [*Olson and Pfitzer*, 1982]. The numerical t_b curves were calculated using a Python wrapper for IRBEM. It traces the magnetic field line between mirror points, to calculate t_b assuming conservation of energy and the first adiabatic invariant for locally mirroring electrons.

4 Discussion

The scale sizes reported in section 3.2 are a lower bound. They are similar to the latitudinal scale size reported in *Blake et al.* [1996], and scale size reported in *Parks* [1967]. Furthermore, the latitudinal scale size in this study is roughly $\sim$ 2.6 times larger than other simultaneous microbursts reported in *Crew et al.* [2016] and $\sim$ 10 times larger than than reported in *Dietrich et al.* [2010].

From section 3.2, the microburst scale size at the magnetic equator is similar to the whistler-mode chorus source scale sizes reported in *Agapitov et al.* [2011, 2017]. In *Agapitov et al.* [2011], chorus source scale scales of $\sim$ 600 km were observed by CLUSTER at $L \sim$ 4.5. In *Agapitov et al.* [2017], The Van Allen Probes were used to measure source scale sizes of $\sim$ 500 and $\sim$ 800 km for upper and lower band chorus, respectively. Using the evidence from this analysis, this microburst was most likely scattered by a whistler-mode chorus.

Using the fit parameters from section 3.3, the exponential E-folding energy, E_0 is calculated to be $E_0 \sim 100\ keV$. This is similar to the results in *Lee et al.* [2005] who used STSAT-1 and *Datta et al.* [1997] who used a sounding rocket. It is soft for a typical microburst observed with FIREBIRD-II. Since the electron flux is falling quickly with energy, the majority of electrons seen in the fourth energy channel will be at the lower end of its energy range. Thus the lower bound of the LEO scale size (555 keV electrons), with their lower drift velocity, more realistically represents the microburst size. There is no statistically significant change in E_0 for subsequent bounces.

Lastly, the fitted, high energy t_b shown in Fig. 3 agree well to most models but T04 has the largest discrepancy at lower energies. To get an estimate of the L shell discrepancy ΔL, the spacecraft position for T04 is adjusted to give better agreement with the observed t_b.

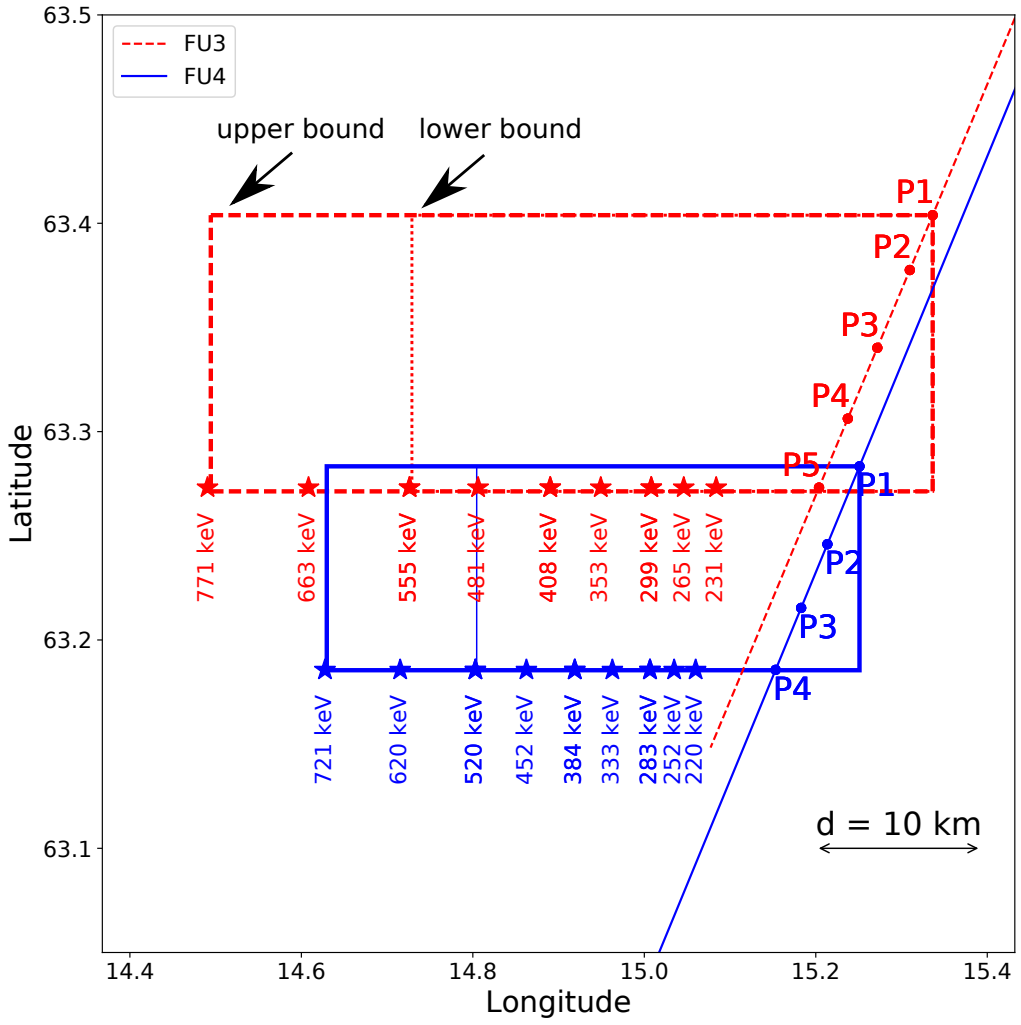

Figure 2. The topology of the FIREBIRD-II orbit and the bouncing packet microburst projected onto latitude and longitude with axis scaled to equal distance. Attributes relating to FU3 shown in red dashed lines, and FU4 with blue solid lines. The spacecraft path is shown with the diagonal lines, starting at the upper right corner. The labels P(N) indicate where the spacecraft were when the N^{th} peak was seen in the lowest energy channel in the HiRes data. The stars with the accompanying energy labels represent the locations of the electrons with that energy that started at time of P1, and were seen at the last peak on each spacecraft. The thick (thin) box represents the upper (lower) bound on the microburst scale size, assuming that the majority of the electrons were in the upper (lower) boundary of energy channel 4.

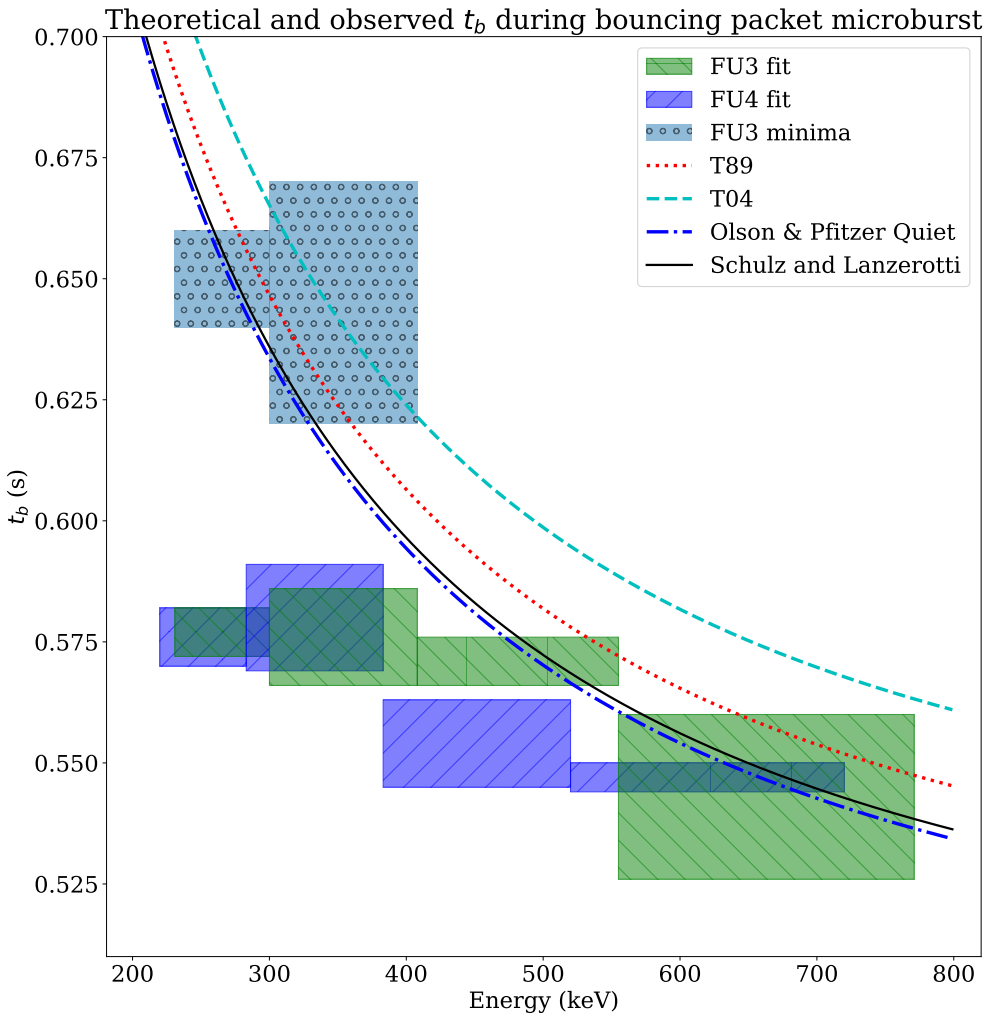

Figure 3. Observed and theoretical t_b for electrons of energies from 200 to 770 keV. The solid black line is t_b in a dipole magnetic field, derived in *Schulz and Lanzerotti* [1974]. The red and cyan dashed lines are the t_b derived using the T89, and T04 magnetic field models with IRBEM. Lastly, the blue dashed curve is the t_b derived using the Olson & Pfitzer Quiet model. The green and purple boxes represent the observed t_b for FU3 and FU4 using a Gaussian fit, respectively. The blue boxes represent the observed t_b calculated with the minima between the bounces. The width of the boxes represent the width of those energy channels, and the height represents the uncertainty from the fit.

The adjusted L shell is smaller by $\Delta L = 0.35$. On the other hand, the t_b calculated using the minima in the lowest two energy channels has much better agreement.

5 Conclusions

The bouncing packet microburst observed by both FIREBIRD-II CubeSats shed light on the spatial and temporal properties of microbursts in LEO and the magnetic equator region. It's calculated latitudinal scale size is greater than 28.8 ± 0.8 km and the longitudinal scale size greater than 8.5 ± 8.8 km at LEO, assuming a soft energy spectra. Using the T89 magnetic field model, these scale sizes were mapped to the magnetic equator. The radial scale size is greater than 504 ± 14 km and azimuthal scale size is greater than 451 ± 103 km, assuming a soft energy spectra. The similarity of the derived microburst equatorial scale size to the whistler-mode chorus source region scale size, magnetospheric location, and geomagnetic conditions indicate that the microburst electrons were probably scattered by a whistler-mode chorus wave.

Lastly, the observed and theoretical bounce periods agree at high energies, but disagree by as much as ~ 20% at the lowest energies that FIREBIRD-II observes. This is partially due to the bias to earlier times in the peaks for the two lowest energy channels, and it hints at the underlying energy-dependent electron flux in those energy channels. By using the minima method to calculate t_b, it is in better agreement for those energy channels.

These rsults will be useful for future modeling efforts in areas not limited to: estimating instanteneous loss rate from the radiation belts, magnetic field modeling, and the scale sizes relationship between waves and microbursts. The scale sizes reported in this study are a lower bound, and from previous literature, it is obvious that there is a distribution of microburst scale sizes. A robust distribution cannot be derived from FIREBIRD-II, since they separated quickly in-track, and observed a small number of coincident microbursts. A follow up study is planned and a similar analysis will be applied to those microbursts, as well as to microbursts observed with the Aerocube 6 CubeSats.

Acknowledgments

I acknowledge the FIREBIRD team, and the members of the Space Sciences and Engineering Laboratory at MSU for their hard work to make this mission a success. In addition, I acknowledge Drew Turner for his suggestions regarding the bounce period calculations. This material is based upon work at Montana State University supported by the National Science Foundation under Grant Numbers 0838034 and 1339414.

References

Abel, B., and R. M. Thorne (1998), Electron scattering loss in earth's inner magnetosphere: 1. dominant physical processes, *Journal of Geophysical Research: Space Physics*, *103*(A2), 2385–2396.

Agapitov, O., V. Krasnoselskikh, T. Dudok de Wit, Y. Khotyaintsev, J. S. Pickett, O. Santolik, and G. Rolland (2011), Multispacecraft observations of chorus emissions as a tool for the plasma density fluctuations' remote sensing, *Journal of Geophysical Research: Space Physics*, *116*(A9), n/a–n/a, doi:10.1029/2011JA016540, a09222.

Agapitov, O., L. W. Blum, F. S. Mozer, J. W. Bonnell, and J. Wygant (2017), Chorus whistler wave source scales as determined from multipoint van allen probe measurements, *Geophysical Research Letters*, pp. n/a–n/a, doi:10.1002/2017GL072701, 2017GL072701.

Anderson, B., S. Shekhar, R. Millan, A. Crew, H. Spence, D. Klumpar, J. Blake, T. O'Brien, and D. Turner (2017), Spatial scale and duration of one microburst region on 13 august 2015, *Journal of Geophysical Research: Space Physics*.

Anderson, K. A., and D. W. Milton (1964), Balloon observations of x rays in the auroral zone: 3. high time resolution studies, *Journal of Geophysical Research*, *69*(21), 4457–4479, doi:10.1029/JZ069i021p04457.

Blake, J., M. Looper, D. Baker, R. Nakamura, B. Klecker, and D. Hovestadt (1996), New high temporal and spatial resolution measurements by sampex of the precipitation of relativistic electrons, *Advances in Space Research*, *18*(8), 171 – 186, doi: http://dx.doi.org/10.1016/0273-1177(95)00969-8.

Blake, J. B., and T. P. O'Brien (2016), Observations of small-scale latitudinal structure in energetic electron precipitation, *Journal of Geophysical Research: Space Physics*, *121*(4), 3031–3035, doi:10.1002/2015JA021815, 2015JA021815.

Blum, L., X. Li, and M. Denton (2015), Rapid mev electron precipitation as observed by sampex/hilt during high-speed stream-driven storms, *Journal of Geophysical Research: Space Physics*, *120*(5), 3783–3794, doi:10.1002/2014JA020633, 2014JA020633.

Crew, A. B., H. E. Spence, J. B. Blake, D. M. Klumpar, B. A. Larsen, T. P. O'Brien, S. Driscoll, M. Handley, J. Legere, S. Longworth, K. Mashburn, E. Mosleh, N. Ryhajlo, S. Smith, L. Springer, and M. Widholm (2016), First multipoint in situ observations of electron microbursts: Initial results from the nsf firebird ii mission, *Journal of Geophysical Research: Space Physics*, *121*(6), 5272–5283, doi:10.1002/2016JA022485, 2016JA022485.

Datta, S., R. Skoug, M. McCarthy, and G. Parks (1997), Modeling of microburst electron precipitation using pitch angle diffusion theory, *Journal of Geophysical Research: Space Physics*, *102*(A8), 17,325–17,333.

Dietrich, S., C. J. Rodger, M. A. Clilverd, J. Bortnik, and T. Raita (2010), Relativistic microburst storm characteristics: Combined satellite and ground-based observations, *Journal of Geophysical Research: Space Physics*, *115*(A12).

Hoots, F. R., and R. L. Roehrich (1980), Models for propagation of norad element sets, *Tech. Rep. 3*, Spacetrack.

Horne, R. B., and R. M. Thorne (2003), Relativistic electron acceleration and precipitation during resonant interactions with whistler-mode chorus, *Geophysical Research Letters*, *30*(10), n/a–n/a, doi:10.1029/2003GL016973, 1527.

Lee, J.-J., G. K. Parks, K. W. Min, H. J. Kim, J. Park, J. Hwang, M. P. McCarthy, E. Lee, K. S. Ryu, J. T. Lim, E. S. Sim, H. W. Lee, K. I. Kang, and H. Y. Park (2005), Energy spectra of 170-360 kev electron microbursts measured by the korean stsat-1, *Geophysical Research Letters*, *32*(13), doi:10.1029/2005GL022996, l13106.

Li, W., R. M. Thorne, V. Angelopoulos, J. Bortnik, C. M. Cully, B. Ni, O. LeContel, A. Roux, U. Auster, and W. Magnes (2009), Global distribution of whistler-mode chorus waves observed on the themis spacecraft, *Geophysical Research Letters*, *36*(9), n/a–n/a, doi:10.1029/2009GL037595, l09104.

Lorentzen, K. R., J. B. Blake, U. S. Inan, and J. Bortnik (2001a), Observations of relativistic electron microbursts in association with vlf chorus, *Journal of Geophysical Research: Space Physics*, *106*(A4), 6017–6027, doi:10.1029/2000JA003018.

Lorentzen, K. R., M. D. Looper, and J. B. Blake (2001b), Relativistic electron microbursts during the gem storms, *Geophysical Research Letters*, *28*(13), 2573–2576, doi: 10.1029/2001GL012926.

Millan, R., and R. Thorne (2007), Review of radiation belt relativistic electron losses, *Journal of Atmospheric and Solar-Terrestrial Physics*, *69*(3), 362 – 377, doi: http://dx.doi.org/10.1016/j.jastp.2006.06.019, global Aspects of Magnetosphere-Ionosphere CouplingGlobal Aspects of Magnetosphere-Ionosphere Coupling.

Nakamura, R., D. N. Baker, J. B. Blake, S. Kanekal, B. Klecker, and D. Hovestadt (1995), Relativistic electron precipitation enhancements near the outer edge of the radiation belt, *Geophysical Research Letters*, *22*(9), 1129–1132, doi:10.1029/95GL00378.

Nakamura, R., M. Isowa, Y. Kamide, D. Baker, J. Blake, and M. Looper (2000), Observations of relativistic electron microbursts in association with vlf chorus, *J. Geophys. Res*, *105*, 15,875–15,885.

O'Brien, T. P., K. R. Lorentzen, I. R. Mann, N. P. Meredith, J. B. Blake, J. F. Fennell, M. D. Looper, D. K. Milling, and R. R. Anderson (2003), Energization of relativistic electrons in the presence of ulf power and mev microbursts: Evidence for dual ulf and vlf acceleration, *Journal of Geophysical Research: Space Physics*, *108*(A8), n/a–n/a, doi: 10.1029/2002JA009784, 1329.

O'Brien, T. P., M. D. Looper, and J. B. Blake (2004), Quantification of relativistic electron microburst losses during the gem storms, *Geophysical Research Letters*, *31*(4), n/a–n/a, doi:10.1029/2003GL018621, l04802.

Oliven, M. N., and D. A. Gurnett (1968), Microburst phenomena: 3. an association between microbursts and vlf chorus, *Journal of Geophysical Research*, *73*(7), 2355–2362, doi: 10.1029/JA073i007p02355.

Olson, W. P., and K. A. Pfitzer (1982), A dynamic model of the magnetospheric magnetic and electric fields for july 29, 1977, *Journal of Geophysical Research: Space Physics*, *87*(A8), 5943–5948, doi:10.1029/JA087iA08p05943.

Parks, G. (2003), *Physics Of Space Plasmas: An Introduction, Second Edition*, Westview Press.

Parks, G. K. (1967), Spatial characteristics of auroral-zone x-ray microbursts, *Journal of Geophysical Research*, *72*(1), 215–226.

Schulz, M., and L. J. Lanzerotti (1974), *Particle Diffusion in the Radiation Belts*, Springer.

Selesnick, R. S., J. B. Blake, and R. A. Mewaldt (2003), Atmospheric losses of radiation belt electrons, *Journal of Geophysical Research: Space Physics*, *108*(A12), doi: 10.1029/2003JA010160, 1468.

Shprits, Y. Y., and R. M. Thorne (2004), Time dependent radial diffusion modeling of relativistic electrons with realistic loss rates, *Geophysical Research Letters*, *31*(8), n/a–n/a, doi:10.1029/2004GL019591, l08805.

Shprits, Y. Y., N. P. Meredith, and R. M. Thorne (2007), Parameterization of radiation belt electron loss timescales due to interactions with chorus waves, *Geophysical Research Letters*, *34*(11), n/a–n/a, doi:10.1029/2006GL029050, l11110.

Thorne, R. M. (2010), Radiation belt dynamics: The importance of wave-particle interactions, *Geophysical Research Letters*, *37*(22), doi:10.1029/2010GL044990, l22107.

Thorne, R. M., T. P. O'Brien, Y. Y. Shprits, D. Summers, and R. B. Horne (2005), Timescale for mev electron microburst loss during geomagnetic storms, *Journal of Geophysical Research: Space Physics*, *110*(A9), n/a–n/a, doi:10.1029/2004JA010882, a09202.

Tsyganenko, N. (1989), A solution of the chapman-ferraro problem for an ellipsoidal magnetopause, *Planetary and Space Science*, *37*(9), 1037 – 1046, doi: http://dx.doi.org/10.1016/0032-0633(89)90076-7.

Tsyganenko, N. A., and M. I. Sitnov (2005), Modeling the dynamics of the inner magnetosphere during strong geomagnetic storms, *Journal of Geophysical Research: Space Physics*, *110*(A3), n/a–n/a, doi:10.1029/2004JA010798, a03208.

Ukhorskiy, A. Y., B. J. Anderson, P. C. Brandt, and N. A. Tsyganenko (2006), Storm time evolution of the outer radiation belt: Transport and losses, *Journal of Geophysical Research: Space Physics*, *111*(A11), n/a–n/a, doi:10.1029/2006JA011690, a11S03.

Woodger, L., A. Halford, R. Millan, M. McCarthy, D. Smith, G. Bowers, J. Sample, B. Anderson, and X. Liang (2015), A summary of the barrel campaigns: Technique for studying electron precipitation, *Journal of Geophysical Research: Space Physics*, *120*(6), 4922–4935.